

## Gas temperature measurements using wavelength modulation spectroscopy at 1.39 $\mu\text{m}$

TINGDONG CAI<sup>1\*</sup>, TU TAN<sup>1</sup>, GUISHI WANG<sup>1</sup>, WEIDONG CHEN<sup>2</sup>, XIAOMING GAO<sup>1\*</sup>

<sup>1</sup>Anhui Institute of Optics and Fine Mechanics, the Chinese Academy of Sciences, Hefei 230031, P.R. China

<sup>2</sup>Laboratoire de Physicochimie de l'Atmosphère, Université du Littoral Côte d'Opale 189A, Av. Maurice Schumann, 59140 Dunkerque, France

\*Corresponding authors: Tingdong Cai – caitingdong@126.com, Xiaoming Gao – xmgao@aiofm.ac.cn

Gas temperature measurements in a combustion system by using wavelength modulation spectroscopy  $2f$  ratio of two selected transitions method were presented for 1.39  $\mu\text{m}$ . Wavelength modulation was performed at 35 kHz, and was superimposed on 500 Hz wavelength scans in order to recover full second-harmonic line shapes.  $\text{H}_2\text{O}$  line-pair at 7164.901  $\text{cm}^{-1}$  and 7165.215  $\text{cm}^{-1}$  was selected for this measurement. The criteria of the line-pair selection were discussed. The sensitivity and accuracy of the sensor were demonstrated in a static cell in laboratory (over the temperature range of 400–1000 K, average bias  $\sigma_T \sim 5$  K). Burner experiments demonstrate the ability of our system for *in situ* measurements. The influence caused by variation of total pressure and species concentration in burning gas during combustion was also discussed.

Keywords: combustion, gas temperature measurements, wavelength modulation spectroscopy, water vapor.

### 1. Introduction

Measurements of time-varying gas temperature are important for the combustion efficiency of some industrial processes such as ferrous metallurgy, aerospace, petrochemical industry, electric power, and so on. Thermocouples are traditionally used to measure gas temperature for this application. However, thermocouple probes provide only point measurements with typically a sub-Hz time response.

Laser absorption spectroscopy can provide a fast, sensitive, non-intrusive, and reliable method for *in situ* measurements of multiple flow-field parameters such as temperature, concentration, pressure and velocity in various harsh environments [1–6]. The use of near-infrared tunable diode lasers (TDL) is attractive since they are compact, available, robust, and compatible with optical fiber technology. Much of the temperature work was focused on atmospheric pressure by direct absorption spectroscopy [7–10] or second harmonic detection ( $2f$ ) of wavelength modulation

spectroscopy (WMS) [11–13]. The ratio of absorbance measurements of two transitions measured by TDL can provide path-averaged gas temperature along the laser beam, which is a better indication of the bulk gas temperature than the point temperature measured by thermocouples typically near the wall. Especially the WMS, due to its increased sensitivity and simplified data analysis, has been used widely.

In this work, the temperature is measured by the WMS-2*f* ratio of two H<sub>2</sub>O lines. Water vapor (H<sub>2</sub>O) is one of the primary hydrocarbon combustion products and has a rich absorption spectrum throughout the infrared. A line pair near 1.396 μm is selected because the overtone and combination bands of H<sub>2</sub>O near 1.4 μm are relatively free of interference from absorption by the major combustion products and commercially available telecommunication fiber-coupled diode lasers and optics are readily available. The fundamental quantitative spectroscopy for the selected lines is carefully measured in a heated cell, temperature measurements are validated in this controlled environment over the expected temperature range of 400 to 1000 K, and a demonstration of its use in a laboratory flame is presented. Through analysis of the experimental data, the influence of the gas pressure and species concentration is also researched.

## 2. Wavelength modulation spectroscopy for temperature measurements

For a diode laser which is injection-current tuned around a fixed central frequency, the momentary frequency  $\nu(t)$  and laser intensity  $I_0(t)$  can be represented by

$$\nu(t) = \bar{\nu} + a \cos(\omega_m t) \quad (1)$$

$$I_0(t) = I_0 + i_0 \cos(\omega_m t + \psi) \quad (2)$$

where  $\nu(t)$  is the instantaneous optical frequency,  $I_0(t)$  is the laser emission intensity, and  $\psi$  is the phase shift between intensity modulation and frequency modulation. The quantities  $\bar{\nu}$  and  $I_0$  are average optical frequency and intensity of the laser;  $a$  (modulation amplitude) and  $i_0$  are the maximum small-amplitude excursions of  $\nu(t)$  and  $I_0(t)$  around  $\bar{\nu}$  and  $I_0$ .

After absorption in a uniform medium, the laser transmitted intensity  $I(t)$  can be related to  $I_0(t)$  by the Beer–Lambert relation

$$I(t) = I_0(t) \tau(\nu(t)) = I_0(t) \exp(-PXS\phi_\nu L) \quad (3)$$

where  $\tau(\nu(t))$  is the transmission coefficient,  $P$  [atm] is the total pressure,  $X$  is the mole fraction of the absorbing species,  $S$  [cm<sup>-2</sup>atm<sup>-1</sup>] is the line strength of the transition,  $\phi_\nu$  [cm] is the line-shape function which is normalized such that  $\int \phi_i(\nu) d\nu \equiv 1$ , and  $L$  [cm] is the length of the homogeneous absorbing medium.

The full expression of the laser transmitted intensity  $I(t)$  impinging on a photo-detector can be obtained by developing the even function of  $\tau(\nu(t)) = \tau(\bar{\nu} + a\cos(\omega_m t))$  in a Fourier cosine series [14]:

$$\tau(\nu(t)) = \sum_{n=0}^{+\infty} H_n(\bar{\nu}, a) \cos(n\omega_m t) \quad (4)$$

The function  $H_n(\bar{\nu}, a)$  is the  $n$ -th Fourier coefficient of the transmission coefficient and can be given by

$$H_0(\bar{\nu}, a) = \frac{1}{2\pi} \int_{-\pi}^{+\pi} \tau(\bar{\nu} + a\cos\theta) d\theta \quad (5)$$

$$H_n(\bar{\nu}, a) = \frac{1}{\pi} \int_{-\pi}^{+\pi} \tau(\bar{\nu} + a\cos\theta) \cos(n\theta) d\theta \quad (6)$$

For optically thin samples,  $PXS\phi_\nu L \ll 1$  (or less than about 0.10), the transmission should be reduced to

$$\tau = \exp(-PXS\phi_\nu L) \approx 1 - PXS\phi_\nu L \quad (7)$$

and the second-harmonic Fourier component which is used most frequently could be simplified [15] as

$$H_2(\bar{\nu}, a) = -\frac{SPXL}{\pi} \int_{-\pi}^{+\pi} \phi(\bar{\nu} + a\cos\theta) \cos(2\theta) d\theta \quad (8)$$

In direct absorption techniques, it has already been well-known that the gas temperature should be measured by the ratio of line strengths of two different temperature-dependent transitions, just as

$$R = \frac{S_1(T)}{S_2(T)} = \frac{S(T_0, \nu_1)}{S(T_0, \nu_2)} \exp\left[-\frac{hc}{k} (E_1'' - E_2'') \left(\frac{1}{T} - \frac{1}{T_0}\right)\right] \quad (9)$$

where  $S(T_0, \nu_i)$  is the line strength of the transition centred at  $\nu_i$  ( $\text{cm}^{-1}$ ) for the reference temperature  $T_0$ ;  $h$  is Planck's constant (Js);  $c$  is the speed of light ( $\text{cm s}^{-1}$ );  $k$  is Boltzmann's constant ( $\text{JK}^{-1}$ );  $E''$  is the lower state energy ( $\text{cm}^{-1}$ ); and  $T$  is the gas temperature (K).

The relative sensitivity of absorption strength ratio to temperature can be obtained by differentiating Eq. (9):

$$\left| \frac{\partial R/R}{\partial T/T} \right| = \frac{hc}{k} \frac{E_1'' - E_2''}{T} \quad (10)$$

Similar to direct absorption techniques, WMS also employs the line-pair method to measure gas temperature. This method can be used to obtain temperature because the WMS- $2f$  peak height ratio of two transitions is a function of temperature, just as the ratio of absorption line strengths, *i.e.*

$$R_{2f} = \frac{H_2(\nu_1)}{H_2(\nu_2)} = \frac{S_1(T)}{S_2(T)} \frac{\int_{-\pi}^{+\pi} \phi(\bar{\nu}_1 + a_1 \cos \theta) \cos(2\theta) d\theta}{\int_{-\pi}^{+\pi} \phi(\bar{\nu}_2 + a_2 \cos \theta) \cos(2\theta) d\theta} \quad (11)$$

From the above equation, it should be seen that the WMS- $2f$  peak height ratio ( $R_{2f}$ ) is not only the function of temperature, but is also related to total pressure, species concentration and modulation depth. These factors make the temperature measurement more complicated, but may be mitigated by setting the modulation amplitude around an optimum value, as discussed in [16], which will be discussed in follow. So in this experiment, the modulation amplitude is fixed around the optimum value, and then the influence of total pressure or species concentration could be studied.

### 3. Water line pair for temperature measurement

In development of the line-pair thermometry using WMS, the selection of an optimum spectral line pair is very important. There is a lot of criterions which could be used for the selection [12, 17, 18]. The line strength of water over a range of wavelengths from 1 to 2  $\mu\text{m}$  at a temperature of 1000 K based on the HITRAN/HITEMP database [19]

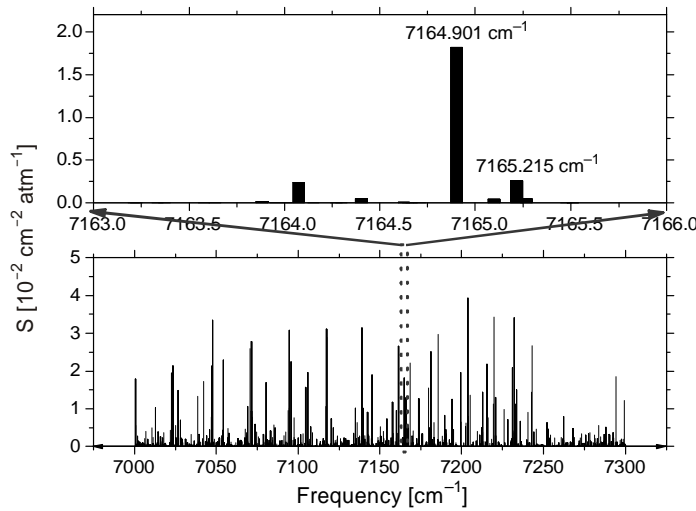


Fig. 1. HITEMP simulation of  $\text{H}_2\text{O}$  absorption spectra at 1000 K from 7000 to 7300  $\text{cm}^{-1}$ .

is graphically depicted in Fig. 1. Based on those information, here two lines located at  $7164.901 \text{ cm}^{-1}$  and  $7165.215 \text{ cm}^{-1}$  are selected as the line pair, and the reasons are as follows.

### 3.1. Position of the line pair

The line pair is located at the region of  $1.39 \mu\text{m}$ , where the  $\nu_1 + \nu_3$  combination band of  $\text{H}_2\text{O}$  absorption spectra overlap with the most common telecommunication bands, thus diode laser and optical fiber in this band are widely available [20].

### 3.2. Line separation of the pair

At present time the typical rapid-tuning range of the telecommunication quality single-mode DFB diode laser commercially available is  $0$  to  $2 \text{ cm}^{-1}$ . Hence the spectral separation of the two transitions must range between  $0.2$  and  $1 \text{ cm}^{-1}$  for a suitable line pair. A bigger line separation will lead the laser intensity not sufficient enough to provide a good signal-to-noise, and a smaller separation will make data analysis more complicated due to the overlap of the two absorption features at atmospheric pressure. Here separation of the pair is  $0.314 \text{ cm}^{-1}$ , so the laser intensity could be sufficient and interference caused by the overlap of the two absorption features also could be avoided.

### 3.3. Absorption strength of the pair

The peak absorbance of a single, isolated  $\text{H}_2\text{O}$  transition is

$$\alpha_{\nu, \text{peak}} = PXS(T) \phi_{\nu, \text{peak}} L \quad (12)$$

where  $\phi_{\nu, \text{peak}}$  is the peak value of line-shape function. An empirical approximation to the Voigt profile [21] is used to calculate the peak value of the line-shape function. The peak absorbance of the pair must be large enough to ensure a good signal-to-noise ratio. We assume a minimum detectable absorbance of  $10^{-4}$ , and a desired SNR of 10, which requires a peak absorption be greater than  $10^{-3}$ . But in order to meet the “weak transition” assumption in (7), associated with wavelength modulation measurements, the peak absorption should be less than  $\sim 0.1$ .

For a path length of  $38 \text{ cm}$  and a combustion product water vapor mole fraction between  $0.01$  to  $0.2$ , typical of hydrocarbon combustion products at a pressure of  $1 \text{ atm}$ , the peak absorbance can be calculated as follows

$$\alpha_{\nu, \text{peak}} = PXS(T) \phi_{\nu, \text{peak}} L = 1 \text{ atm} \times 1\% \times S(T) \times \phi_{\nu, \text{peak}} \times 38 \text{ cm} \geq 10^{-3} \quad (13)$$

$$\alpha_{\nu, \text{peak}} = PXS(T) \phi_{\nu, \text{peak}} L = 1 \text{ atm} \times 20\% \times S(T) \times \phi_{\nu, \text{peak}} \times 38 \text{ cm} \leq 0.1 \quad (14)$$

The constraint on the product of line strength and line-shape function becomes

$$0.0125 \text{ cm}^{-1} \text{ atm}^{-1} \geq S(T) \phi_{\nu, \text{peak}} \geq 0.0026 \text{ cm}^{-1} \text{ atm}^{-1} \quad (15)$$

in the temperature range of 300–2000 K. The value at different temperatures should be calculated by checking the needed parameters in HITRAN and HITEMP database. Through the calculation we can find that the absorption strength of the pair is suitable.

### 3.4. Relation between the ratio of WMS-2*f* signals and temperature

From Equation (11), the ratio of WMS-2*f* signals is closely related to the ratio of the individual line strengths. The relation of line strength and line strength ratio of the selected lines to temperature is shown in Fig. 2. As shown in this figure, the line

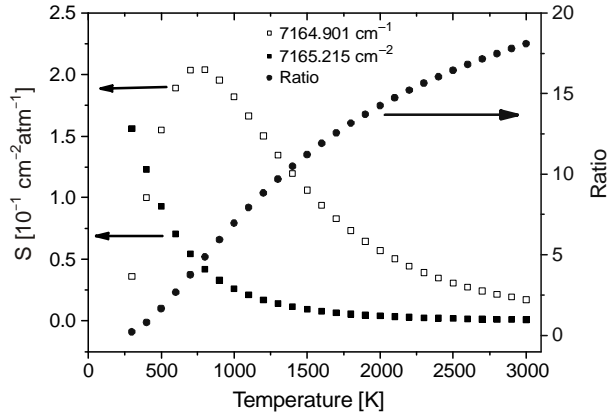


Fig. 2. The relation between line strength and line strength ratio of the selected lines and temperature.

strength ratio is monotone with temperature in the range of 300 to 3000 K. Using the relation between the line strength ratio and temperature, temperature of the gas should be obtained through the measurement of the ratio of WMS-2*f* signals.

### 3.5 Sensitivity of WMS-2*f* signals' ratio to temperature

The uncertainty of the ratio of peak WMS-2*f* signals ( $R_{2f}$ ), represented by standard deviation  $\sigma_{R_{2f}}$ , should be calculated using the error propagation equation [17, 22]:

$$\sigma_{R_{2f}} \equiv \sigma_{H_2(\nu_1)}^2 \left( \frac{\partial R_{2f}}{\partial H_2(\nu_1)} \right)^2 + \sigma_{H_2(\nu_2)}^2 \left( \frac{\partial R_{2f}}{\partial H_2(\nu_2)} \right)^2 + 2 \sigma_{H_2(\nu_1\nu_2)}^2 \frac{\partial R_{2f}}{\partial H_2(\nu_1)} \frac{\partial R_{2f}}{\partial H_2(\nu_2)} \quad (16)$$

The partial derivatives in Eq. (16) are represented as

$$\begin{aligned} \frac{\partial R_{2f}}{\partial H_2(\nu_1)} &= \frac{R_{2f}}{H_2(\nu_1)} \\ \frac{\partial R_{2f}}{\partial H_2(\nu_2)} &= -\frac{R_{2f}}{H_2(\nu_2)} \end{aligned} \quad (17)$$

Assuming the  $2f$  peak heights  $H_2(\nu_1)$  and  $H_2(\nu_2)$  are uncorrelated,  $dR_{2f}/R_{2f}$  can be estimated using

$$\left| \frac{dR_{2f}}{R_{2f}} \right| \approx \frac{\sigma_{R_{2f}}}{R_{2f}} \cong \sqrt{\left( \frac{\sigma_{H_2(\nu_1)}}{H_2(\nu_1)} \right)^2 + \left( \frac{\sigma_{H_2(\nu_2)}}{H_2(\nu_2)} \right)^2} \quad (18)$$

The sensitivity of line strength ratio to temperature is obtained from Eq. (10). It is generally desirable that the temperature sensitivity be as high as possible, resulting in a more accurate sensor.

If the  $2f$  peak heights can be determined within 3%, in order to obtain a temperature accuracy of 5% in the temperature range of 300–1500 K, the constraint on minimum lower state energy difference could be given as follows while the influence of line shape function is neglected

$$|\Delta E''| = |E''_{\nu_1} - E''_{\nu_2}| \geq \left| \frac{dR_{2f}/R}{dT/T} \right| T \frac{hc}{k} = \frac{0.03\sqrt{2}}{0.05} \times 1500 \times \frac{1}{1.4388} = 885 \text{ cm}^{-1} \quad (19)$$

Here the lower state energy difference of the selected line pair is

$$|\Delta E''| = |E''_1 - E''_2| = 995.36 \text{ cm}^{-1} \quad (20)$$

### 3.6. Influence of a cold boundary layer

The difference of integrated absorbance along the beam path in the boundary layer can be used to evaluate the impact of a cold boundary layer on the measurement accuracy of the uniform core temperature [23]:

$$\begin{aligned} \Delta A &= A_c - A = P_x \left[ S \left( T_c \delta - \int_0^\delta S d\xi \right) \right] = P_x \int_{S_b}^{S_c} \xi dS = \\ &= P_x \frac{hc}{k} \int_{T_b}^{T_c} \xi S(T) \frac{E'' - E(T)}{T^2} dT \end{aligned} \quad (21)$$

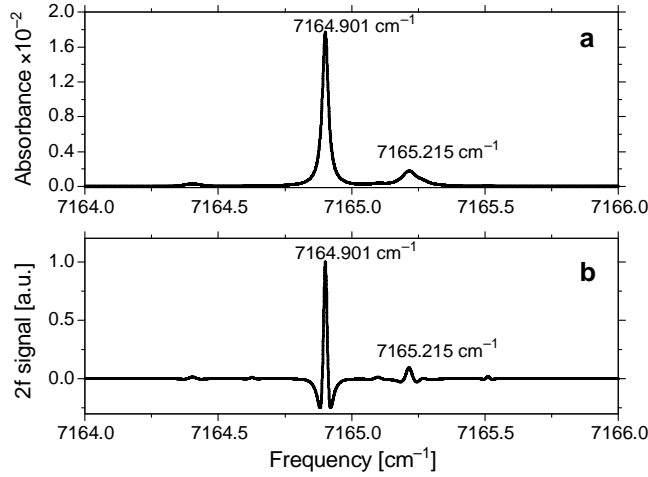
where  $A$  is the integrated absorbance caused by boundary layer water vapor,  $\delta$  is the boundary layer thickness,  $\xi$  is the spatial integration variable, the subscript  $b$  denotes quantities evaluated at the boundary temperature and  $c$  labels quantities evaluated at the uniform core temperature, and  $E(T)$  is a characteristic energy of the absorbing species and depends on temperature [23]:

$$E(T) = \frac{k}{hc} \frac{T}{Q(T)} \frac{d[TQ(T)]}{dT} \quad (22)$$

where  $Q(T)$  is the partition function of the absorbing molecule.

T a b l e. Spectral parameters of the two selected H<sub>2</sub>O lines at 1000 K.

Line position [cm <sup>-1</sup> ]	Line intensity at 1000 K [cm <sup>-2</sup> atm <sup>-1</sup> ]	Self broadening coefficient $\gamma_{\text{self}}$ [cm <sup>-1</sup> ]	Air broadening coefficient $\gamma_{\text{air}}$ [cm <sup>-1</sup> ]
7164.901	$1.819 \times 10^{-2}$	0.2000	0.0161
7165.215	$2.612 \times 10^{-3}$	0.4650	0.0396

Fig. 3. Simulated signal for the selected H<sub>2</sub>O line pair using HITRAN 2004 database for  $P = 1$  atm, 10% H<sub>2</sub>O in air,  $T = 1000$  K: direct absorption signal (a);  $2f$  signal (b).

As can be seen from Eq. (21), the boundary layer does not influence the temperature measurement while  $\Delta A \ll A$ , hence the lower state energy  $E''$  must be much bigger than the characteristic energy of the absorbing species  $E(T)E_{\text{H}_2\text{O}}(T)$  range from 431 to 3023 cm<sup>-1</sup> in the temperature range of 300–1500 K, therefore the lower state energy  $E''$  of the selected lines must be bigger than 300 cm<sup>-1</sup>. Here the influence of the cold boundary layer should be neglected because  $E''$  of the selected line pair meets this condition; they are 1394.81 cm<sup>-1</sup> and 399.46 cm<sup>-1</sup>, respectively.

Figure 3 shows simulated direct absorption and  $2f$  signal for the selected H<sub>2</sub>O line pair based on the HITRAN 2004 parameters at the temperature 1000 K; the spectral constants are listed in the Table.

#### 4. Demonstration of temperature measurements on a laboratory static cell

Figure 4 illustrates the arrangement employed for the measurement of temperature on a laboratory static cell. Light from a distributed-feedback (DFB) InGaAsP laser (NTT) emitting near 1.39  $\mu\text{m}$  is directed across a heated static cell. The diode laser is temperature and current controlled (ILX Lightwave LDC-3724) and driven by a 500 Hz triangle ramp summed in an adder with a 35 kHz sine wave to provide

Table. Continued.

Temperature exponent $n_{\text{air}}$	Lower state energy [ $\text{cm}^{-1}$ ]
0.59	1394.8142
0.69	399.4575

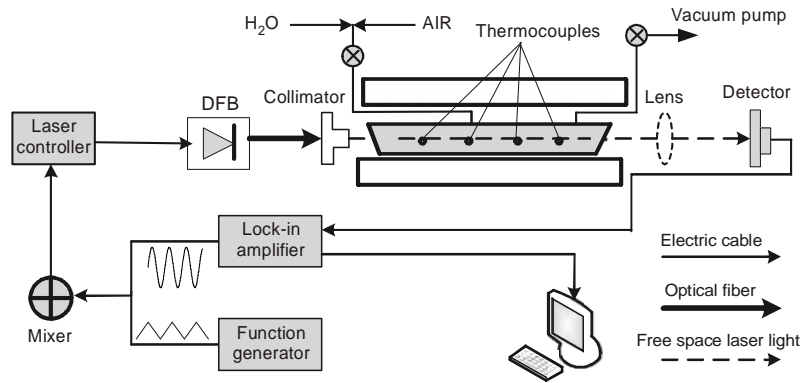


Fig. 4. Experimental setup.

the wavelength modulation. A lock-in amplifier (Model SR-830) is used to measure the second-harmonic component of the transmitted laser signal. The beam path is purged by high-pure nitrogen so as to avoid the interference from ambient water vapor in room air. The gas cell (38 cm long with canted wedged ( $1.5^\circ$ ) windows to avoid residual etalon fringes) is heated by a temperature controller, and the temperature of gas samples is determined by four type-K thermocouples with an accuracy of  $\pm 1\%$  of reading placed equally along the heated cell. At each temperature set point in the range of 400–1000 K, the controller is adjusted to guarantee that the measured deviation of the four thermocouple readings is less than 4 K.

The modulation depth is set at an optimum value so as to mitigate its effect. Figure 5 plots the simulated normalized WMS- $2f$  peak heights of the  $\text{H}_2\text{O}$  line pair versus modulation depth at the temperature of 1000 K. The Voigt line shape with the spectroscopic parameters listed in the Table is used in the numerical simulation. As shown in this figure, the WMS- $2f$  peak height of each line varies slowly at the modulation depth  $a_{\text{opt}} = 0.062 \text{ cm}^{-1}$ . By choosing this value, the integral in (8) should remain relatively constant. Hence the effect of modulation depth on the ratio of two WMS- $2f$  peak heights should be neglected.

The respective  $\text{H}_2\text{O}$  scanned WMS- $2f$  line shapes for the selected line pair measured at different temperature are shown in Fig. 6. As can be seen from the picture, intensities of these WMS- $2f$  signals vary obviously along with the change of temperature. Figure 7 illustrates the  $2f$  peak to peak height and the  $2f$  peak ratio as a function of temperature for the selected  $\text{H}_2\text{O}$  line pair in temperature range of 400–1000 K, and a single data point at 700 K is used to calibrate the WMS- $2f$  sensor. Just as the analysis

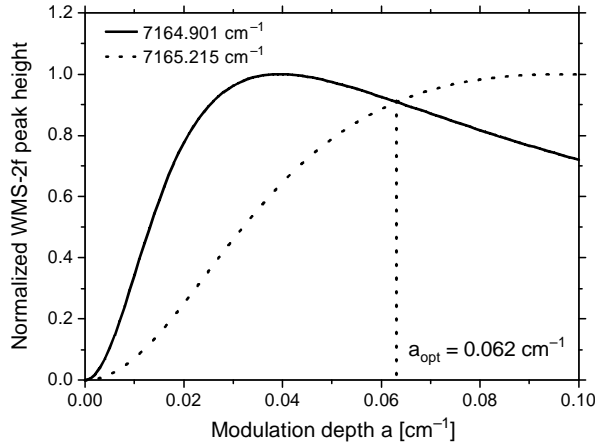


Fig. 5. Simulated WMS- $2f$  peak height for the selected line pair versus modulation depth;  $P = 1$  atm, 1%  $\text{H}_2\text{O}$  in air, and  $L = 38$  cm.

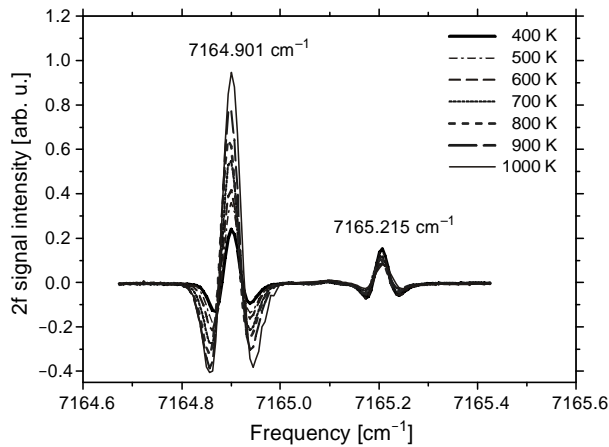


Fig. 6. The  $2f$  signal of the selected line-pair at different temperature.

in Section 3.4, both the heights and ratio are monotonic function of temperature in the needed temperature range. It confirms that the gas temperature could be measured by  $2f$  peak ratio of the selected line pair.

A set of static heated cell experiments with controlled gas mixtures are carried out to validate the WMS- $2f$  sensor thermometry. The  $\text{H}_2\text{O}$ -air mixtures at atmospheric pressure are prepared in a stainless tank by choosing a desired mixture composition. In order to ensure the homogeneous of the mixture, the tank is shaken and allowed to rest for at least 3 hours before the mixture is delivered to the static cell which has been heated to a setting temperature; here two values of water concentration (1% and 10%) are used. Figure 8 shows the comparison between the temperatures from the WMS- $2f$  sensor thermometry and the thermocouple readings. The top and bottom graphs in this

figure show the cases while the value of water concentration is 1% and 10%, respectively. Correlation of those measured points has an  $R^2$  value of 0.9993 and 0.99853, standard deviation is 1.2% and 1.6% (the error bar is too small to resolve), respectively. The results indicate that the temperatures measured by the WMS-2f sensor coincide perfectly with the thermocouple readings over the full temperature range of 400–1000 K (average bias  $\sigma_T = |T_{\text{TDL}} - T_{\text{TC}}| \sim 5$  K). The error in Fig. 8 primarily comes from uncertainties in temperature measurements by thermocouple (1%) and measured spectroscopic data (0.5%). The efficiency and accuracy of the WMS-2f sensor thermometry show its good potential for temperature sensing.

It is well-known that the total pressure and species concentration may be changed during combustion, unfortunately 2f peak ratio is influenced by the two factors as

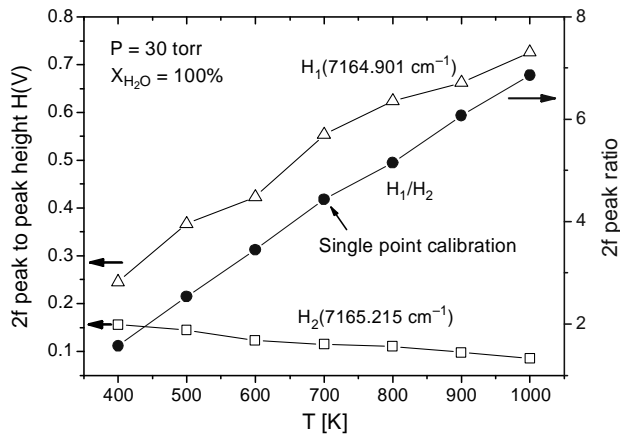


Fig. 7. The 2f peak to peak heights and their ratio of the two transitions at different temperature.

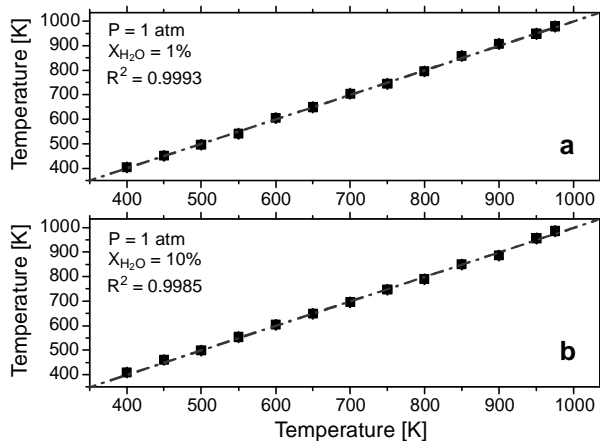


Fig. 8. Comparison of measured temperature with thermocouple temperature with  $\text{H}_2\text{O}$  concentration of 10% (a) and 1% (b).

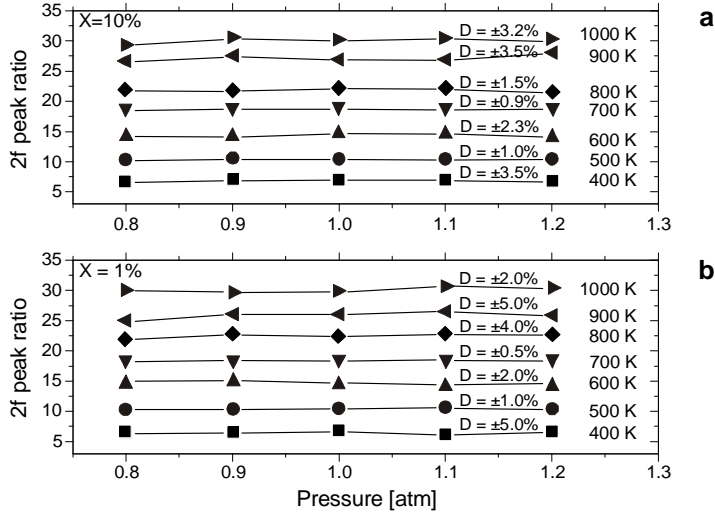


Fig. 9. The ratio of the  $2f$  amplitudes of the two transitions at different total pressures with  $H_2O$  concentration of 10% (a) and 1% (b).

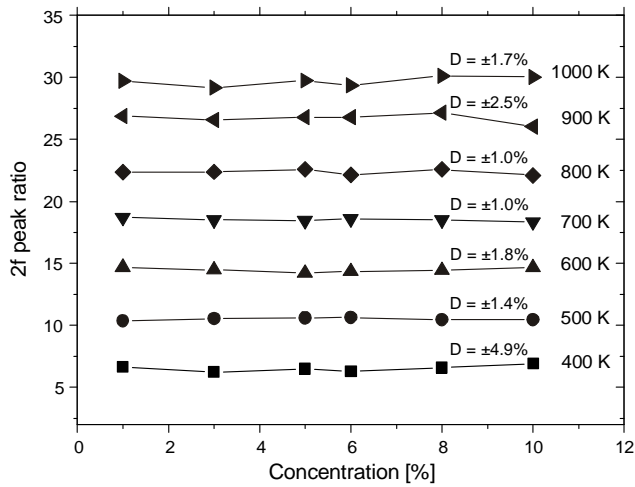


Fig. 10. The ratio of the  $2f$  amplitudes of the two transitions at different  $H_2O$  concentration,  $P = 1$  atm.

the line-shape function  $\phi_v$  is the function of total pressure and species concentration. The impact of the change of the two factors on  $2f$  peak ratio will be discussed in next.

The impact of total pressure on  $2f$  peak ratios in the temperature range of 400–1000 K with  $H_2O$  concentration are 1% and 10%, as is shown in Figs. 9a and 9b, respectively. As illustrated in these graphs, values of the  $2f$  peak ratios at each temperature are nearly the same in pressure range of 0.8–1.2 atm, the biggest deviation of each set of points is  $\pm 5\%$ . It indicates that the small influence of total pressure on  $2f$  peak ratio could be neglected. Figure 10 illustrates the impact of  $H_2O$  concentration

in the same temperature range as above at the experimental condition of  $P = 1$  atm. The influence of the concentration is similar to total pressure. As given in this figure, the biggest deviation of each set of points is only  $\pm 4.9\%$  as the concentration change from 1% to 10%, and the error may be caused partly by thermocouple readings. Hence the impact of  $\text{H}_2\text{O}$  concentration also could be ignored.

## 5. Temperature measurements of combustion gas on a burner

In order to illustrate the potential of the sensor for monitoring the gas temperature in the exhaust of combustion, measurements are made on a burner. The burner can produce a circular uniform flame with a diameter of 12 cm and a height of 1.5 cm. The  $1.39 \mu\text{m}$  single-laser sensor is driven by an external modulation, which consists of a 500 Hz triangle ramp combined with a faster 35 kHz sinusoidal signal. The beam path is purged to avoid interference from ambient water vapor. The second harmonic components of the transmitted laser signal are obtained by a lock-in amplifier (Model SR-830) with a time constant of  $10 \mu\text{s}$ . A laboratory code is written in LabView for data acquisition and analysis. Figure 11 show the representative WMS- $2f$  signal obtained along middle axle of the flame at some heights above the burner. Once the acquisition is completed, the signal processing program transfers the captured data from on-board memory to PC memory. Data analysis, including peak finding and ratio calculation, is then performed on the accumulated data. The single-point calibration in the heated cell could be used to convert the  $2f$  peak ratio to temperature.

For calibrating the temperature obtained by  $2f$  peak ratio, the thermocouple is traversed forward and back to confirm stability of the flame temperature. The combustion flows of the type studied here should be sufficient to assume an approximate temperature distribution in reducing the data. Comparison of the temperatures from the WMS- $2f$  sensor thermometry with the thermocouple readings in the flame is shown

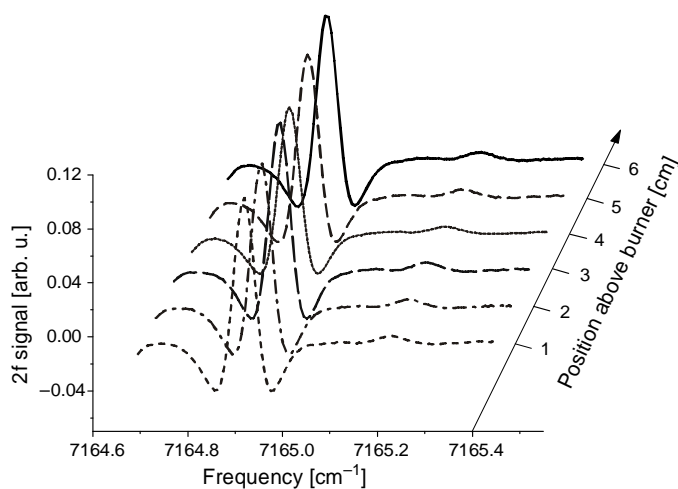


Fig. 11. Representative WMS- $2f$  signal obtained in  $\text{C}_3\text{H}_8/\text{air}$  flame.

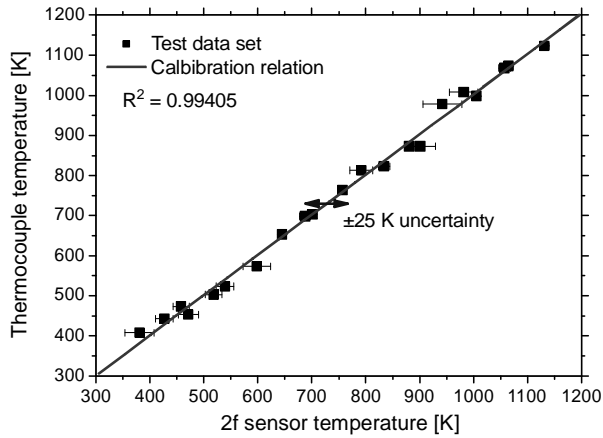


Fig. 12. Comparison of the temperatures from the WMS- $2f$  sensor thermometry with the thermocouple readings in the  $C_3H_8$ /air flame.

in Fig. 12. These test data are all in the error range of  $\pm 25$  K. Correlation of those measured points has an  $R^2$  value of 0.994, the standard deviation is 3%, which shows the perfect performance of the temperature sensor. The error in this figure primarily comes from uncertainties in the measured spectroscopic data, temperature measurements by thermocouple, approximation of the uniform temperature assumption and combustion problem such as instability suppression.

We acquire the distributed profile of temperature in the flame by moving the laser and detector from one side to the other with a step length of 1 cm along the horizontal direction to probe the burned gas 1 cm above the burner surface, the same measurement is done at each height of 2 to 6 cm above the burner surface with a step length of 1 cm.

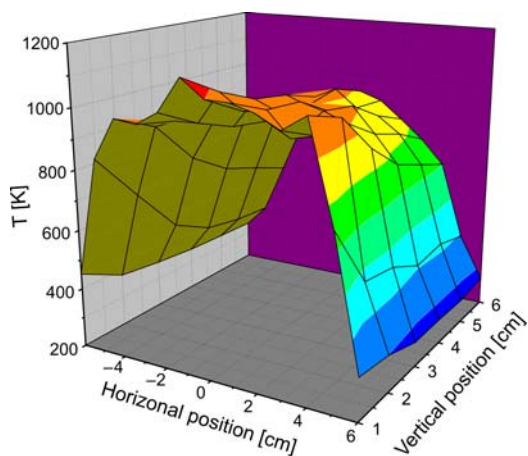


Fig. 13. Distributed profile of temperature in the flame measured by the WMS- $2f$  sensor.

The profile is shown in Fig. 13. As can be inferred from the graph, the cross-section of the temperature profile has a trapezoidal shape. This indicates that temperature in the flame becomes higher gradually from the edge to center at each height and becomes lower as away from the flame in vertical direction. This distributed profile of the temperature obtained by the WMS-2*f* sensor meets the real routine of temperature in a flame. These results demonstrate the utility of this fast temperature sensor for applications to real-time combustion sensing and control.

It should be noted that the present sensor provides accurate temperature for situations in which the temperature distribution along the beam path is uniform or approximately uniform. Under other condition where temperature changes significantly and the relative temperature profile is unknown, it may be attractive to consider multi-line thermometry [24]. Note that the selected line pair is immune to the influence of cold boundary layers, just as the description in 3.6, which will mitigate the temperature error for typical combustion. Also note that a rapid measurement of relative temperature change is more important than determination of an absolute value while dealing with combustion problems such as instability suppression or lean-blow-off. Hence the two-line temperature sensor can provide a potentially useful control variable even for condition with significant temperature gradient.

## 6. Conclusions

A single-diode-laser sensor based on wavelength modulation spectroscopy techniques in H<sub>2</sub>O vapor is developed, validated in a controlled laboratory environment, and demonstrated in a combustion gas. The H<sub>2</sub>O transitions at 7164.901 cm<sup>-1</sup> and 7165.215 cm<sup>-1</sup> are identified as the best line pair through the considerations of proper position and separation, appropriated absorption strength, the monotone relation between ratio of WMS-2*f* signals and temperature, sufficient temperature sensitivity and adequate immunity to the effect of cold boundary layers. These considerations also could be used as lines selection criteria. Laboratory experiments in a static cell were conducted to examine the temperature-sensing capability and accuracy of the two-line sensor. Good agreement between temperatures from the WMS-2*f* sensor thermometry and thermocouple readings shows the sensitivity and accuracy of the sensor. Experiments with real flames on a burner confirmed the utility of the sensor to monitor on-line temperatures and the potential application to combustion control. The influence caused by variation of total pressure and species concentration in burning gas during combustion could be ignored.

*Acknowledgements* – This research was funded by the National 863 High Technology Research and Development Program of China under Grant no. 2006AA06Z237, and the French International Programme of Scientific Cooperation (CNRS/PICS no. 3359). The authors are most grateful to Dr. Weixiong Zhao, Dr. Zhensong Cao and Dr. Jinsong Li for their help in some stages of this work, for helpful discussion and for useful recommendations.

## References

- [1] SONNENFROH D.M., ALLEN M.G., *Observation of CO and CO<sub>2</sub> absorption near 1.57 μm with an external-cavity diode laser*, Applied Optics **36**(15), 1997, pp. 3298–3300.
- [2] SHAO J., GAO X.M., DENG L., HUANG W., YANG Y., PEI S.X., YUAN Y.Q., ZHANG W.J., *Research on absorption spectroscopy of CH<sub>4</sub> around 1.315 μm*, Optica Applicata **35**(1), 2005, pp. 155–162.
- [3] JEFFRIES J.B., SCHULZ C., MATTISON D.W., OEHLSCHLAEGER M.A., BESSLER W.G., LEE T., DAVIDSON D.F., HANSON R.K., *UV absorption of CO<sub>2</sub> for temperature diagnostics of hydrocarbon combustion applications*, Proceedings of the Combustion Institute **30**(1), 2005, pp. 1591–1599.
- [4] MIHALCEA R.M., BAER D.S., HANSON R.K., *Diode laser sensor for measurements of CO, CO<sub>2</sub>, and CH<sub>4</sub> in combustion flows*, Applied Optics **36**(33), 1997, pp. 8745–8752.
- [5] SILVER J.A., KANE D.J., *Diode laser measurements of concentration and temperature in microgravity combustion*, Measurement Science and Technology **10**(10), 1999, pp. 845–852.
- [6] CHAN K., ITO H., INABA H., FURUYA T., *10 km-long fibre-optic remote sensing of CH<sub>4</sub> gas by near infrared absorption*, Applied Physics B **38**(1), 1985, pp. 11–15.
- [7] ROCCO A., DE NATALE G., DE NATALE P., GAGLIARDI G., GIANFRANI L., *A diode-laser-based spectrometer for in-situ measurements of volcanic gases*, Applied Physics B **78**(2), 2004, pp. 235–240.
- [8] WANG J., MAIOROV M., JEFFRIES J.B., GARBUZOV D.Z., CONNOLLY J.C., HANSON R.K., *A potential remote sensor of CO in vehicle exhausts using 2.3 μm diode lasers*, Measurement Science and Technology **11**(11), 2000, pp. 1576–1584.
- [9] LIU X., JEFFRIES J.B., HANSON R.K., HINCKLEY K.M., WOODMANSEE M.A., *Development of a tunable diode laser sensor for measurements of gas turbine exhaust temperature*, Applied Physics B **82**(3), 2006, pp. 469–478.
- [10] MIHALCEA R.M., BAER D.S., HANSON R.K., *A diode-laser absorption sensor system for combustion emission measurements*, Measurement Science and Technology **9**(3), 1998, pp. 327–338.
- [11] UEHARA K., *Dependence of harmonic signals on sample-gas parameters in wavelength-modulation spectroscopy for precise absorption measurements*, Applied Physics B **67**(4), 1998, pp. 517–523.
- [12] ZHOU X., JEFFRIES J.B., HANSON R.K., *Development of a fast temperature sensor for combustion gases using a single tunable diode laser*, Applied Physics B **81**(5), 2005, pp. 711–722.
- [13] GABRYSCH M., CORSI C., PAVONE F.S., INGUSCIO M., *Simultaneous detection of CO and CO<sub>2</sub> using a semiconductor DFB diode laser at 1.578 μm*, Applied Physics B **65**(1), 1997, pp. 75–79.
- [14] PHILIPPE L.C., HANSON R.K., *Laser diode wavelength-modulation spectroscopy for simultaneous measurement of temperature, pressure and velocity in shock-heated oxygen flows*, Applied Optics **32**(30), 1993, pp. 6090–6103.
- [15] NAGALI V., CHOU S.I., BAER D.S., HANSON R.K., *Diode-laser measurements of temperature-dependent half-widths of H<sub>2</sub>O transitions in the 1.4 μm region*, Journal of Quantitative Spectroscopy and Radiative Transfer **57**(6), 1997, pp. 795–809.
- [16] LIU J.T.C., JEFFRIES J.B., HANSON R.K., *Wavelength modulation absorption spectroscopy with 2f detection using multiplexed diode lasers for rapid temperature measurements in gaseous flows*, Applied Physics B **78**(3–4), 2004, pp. 503–511.
- [17] ZHOU X., LIU X., JEFFRIES J.B., HANSON R.K., *Development of a sensor for temperature and water concentration in combustion gases using a single tunable diode laser*, Measurement Science and Technology **14**(8), 2003, pp. 1459–1468.
- [18] ZHOU X., LIU X., JEFFRIES J.B., HANSON R.K., *Selection of NIR H<sub>2</sub>O absorption transitions for in-cylinder measurement of temperature in IC engines*, Measurement Science and Technology **16**(12), 2005, pp. 2437–2445.
- [19] ROTHMAN L.S., JACQUEMART D., BARBE A., CHRIS BENNER D., BIRK M., BROWN L.R., CARLEER M.R., CHACKERIAN JR. C., CHANCE K., COUDERT L.H., DANA V., DEVI V.M., FLAUD J.-M., GAMACHE R.R., GOLDMAN A., HARTMANN J.-M., JUCKS K.W., MAKI A.G., MANDIN J.-Y., MASSIE S.T., ORPHAL J., PERRIN A., RINSLAND C.P., SMITH M.A.H., TENNYSON J., TOLCHENOV R.N., TOTH R.A., VANDER

- AUWERA J., VARANASI P., WAGNER G., *The HITRAN 2004 molecular spectroscopic database*, Journal of Quantitative Spectroscopy and Radiative Transfer **96**(2), 2005, pp. 139–204.
- [20] ALLEN M.G., *Diode laser absorption sensors for gas-dynamic and combustion flows*, Measurement Science and Technology **9**(4), 1998, pp. 545–562.
- [21] DRAYSON S.R., *Rapid computation of the Voigt profile*, Journal of Quantitative Spectroscopy and Radiative Transfer **16**(7), 1976, pp. 611–614.
- [22] BEVINGTON P.R., ROBINSON D.K., *Data Reduction and Error Analysis for the Physical Sciences*, McGraw-Hill, New York 1992.
- [23] OUYANG X., VARGHESE P.L., *Selection of spectral lines for combustion diagnostics*, Applied Optics **29**(33), 1990, pp. 4884–4890.
- [24] SANDERS S.T., WANG J., JEFFRIES J.B., HANSON R.K., *Diode-laser absorption sensor for line-of-sight gas temperature distributions*, Applied Optics **40**(24), 2001, pp. 4404–4415.

Received April 7, 2008  
in revised form May 14, 2008